JOURNAL OF AIRCRAFT
Vol. 43, No. 4, July–August 2006

High-Lift Propulsive Airfoil with Integrated Crossflow Fan

Joseph D. Kummer* and Thong Q. Dang†
Syracuse University, Syracuse, New York 13244

DOI: 10.2514/1.17610

A concept for embedding a crossflow fan into a thick wing for lift enhancement and thrust production is proposed. The design places a crossflow fan propulsion system with raised inlet near the trailing edge of the wing. Flow is drawn in from the suction surface, energized, and expelled out the trailing edge. The integration of a crossflow fan within a modified Gottingen 570 airfoil section with 34% thickness to chord ratio is developed and simulated using the commercial CFD software Fluent. Unsteady sliding mesh calculations are used to visualize the flowfield and calculate fan performance and airfoil lift coefficient. The results of the CFD work show that the jet leaving the fan fills up the wake behind the airfoil, whereas the suction effect produced by the fan virtually eliminates flow separation at high angle of attack, yielding very high-lift coefficients. A system level analysis demonstrates the benefits of using an embedded crossflow fan for distributed aircraft propulsion. The system analysis yields tradeoffs between various design parameters and provides a basis for preliminary crossflow fan airfoil design.

Nomenclature

A	=	area
C_D	=	airfoil drag coefficient, $D/(0.5\rho U_\infty^2 c)$
C_L	=	airfoil lift coefficient, $L/(0.5\rho U_\infty^2 c)$
C_P	=	power coefficient, Power$/(\rho U_\infty^3 D_f)$
C_T	=	thrust coefficient, $T/(0.5\rho U_\infty^2 D_f)$
CS	=	control surface
c	=	airfoil chord length
D	=	drag per unit span
D_{BL}	=	drag due to boundary layer buildup
D_f	=	crossflow fan diameter
F_x	=	x component of force
H	=	arbitrarily large distance
h_i	=	propulsor inlet height
h_j	=	propulsor outlet height
h_w	=	ingested wake height
$\tilde{h}$	=	nondimensionalized ingested wake height
L	=	lift per unit span
M_∞	=	freestream Mach number
$\dot{m}$	=	mass flow rate per unit span
P_p	=	propulsive power per unit span
P_T	=	total pressure
P_{Ti}	=	total pressure at propulsor inlet
$\bar{P}_{Ti}$	=	mass-weighted total pressure at propulsor inlet
P_∞	=	ambient pressure
p	=	variable
Q	=	flow rate per unit span
Re	=	Reynolds number, $(cU_\infty)/\nu$
r	=	radial distance
T	=	propulsor thrust per unit span
U	=	velocity
U_f	=	fan tip speed
$\tilde{U}_j$	=	nondimensionalized jet velocity, U_j/U_∞
U_w	=	propulsor inlet velocity with wake ingestion
U_x	=	x component of velocity
U_∞	=	velocity in freestream
x	=	x coordinate
y	=	y coordinate
Δ	=	change in value
η_c	=	compression efficiency
η_p	=	propulsive efficiency
η_t	=	total efficiency, $(Q\Delta P_T)/(\Omega\tau)$
μ	=	advance ratio, U_∞/U_f
ν	=	kinematic viscosity
ρ	=	density
ϕ	=	flow coefficient, $Q/(D_f U_f)$
τ	=	fan torque per unit span
Ψ_t	=	total pressure coefficient, $\Delta P_T/(0.5\rho U_f^2)$
Ω	=	fan speed, rad/s

Subscripts

in	=	into control volume
j	=	in jet

Superscript

$'$	=	nonwake ingestion

I. Introduction

THE crossflow fan (CFF), developed in 1893 by Mortier, is used extensively in the heating, ventilation, and air conditioning (HVAC) industry. The fan is usually long in relation to the diameter, so the flow approximately remains 2-dimensional (2-D). The CFF uses an impeller with forward curved blades, placed in a housing consisting of a rear wall and a vortex wall. Unlike radial machines, the main flow moves transversely across the impeller, passing the blading twice. Figure 1 shows a typical HVAC configuration [1].

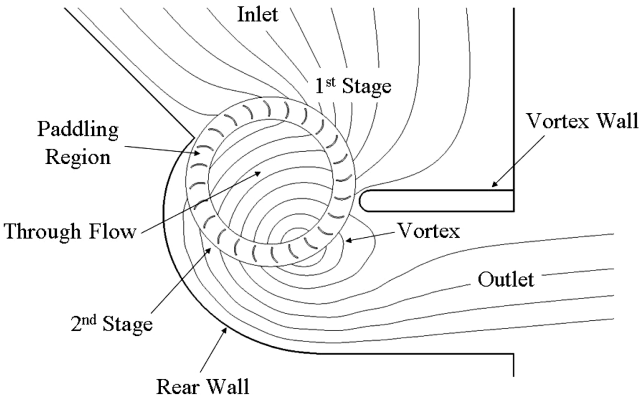

Fig. 1 Diagram of crossflow fan (geometry from [1]).

Received 10 May 2005; revision received 2 November 2005; accepted for publication 24 December 2005.

*University Fellow Graduate Student, Department of Mechanical and Aerospace, 149 Link Hall, AIAA Student Member.

†Professor, Department of Mechanical and Aerospace Engineering, 149 Link Hall, AIAA Member.

Inherent in all designs is a vortex region near the fan discharge, called an eccentric vortex, and a paddling region directly opposite. These regions are dissipative, and as a result, only a portion of the impeller imparts usable work on the flow. The crossflow fan, or transverse fan, is thus a two-stage partial admission machine.

The popularity of the crossflow fan in the HVAC industry comes from its compactness and its ability to provide high-pressure coefficient. Effectively a rectangular fan, the diameter of the crossflow fan readily scales to fit the available space, and the length is adjustable to meet flow rate requirements for the particular application. Because the flow both enters and exits the impeller radially, the crossflow fan is well suited for aircraft embedded distributed-propulsion applications. Because of the 2-D nature of the flow, the fan readily integrates into a wing for use in both thrust production and boundary layer control.

The propulsive wing has several benefits. Smith showed that smoothing of the wake distortion behind a body through ingestion of the viscous wake into an engine reduces the necessary propulsive power [2]. Using an actuator disk theory, Smith demonstrated that it is possible to achieve propulsive efficiencies greater than 1, the theoretical maximum for propulsion without wake ingestion. In the same light, if the engine ingests the boundary layer over the surface of a wing, the same benefit can be realized by reenergizing the low momentum fluid and expelling it out at the trailing edge to fill in the wake. Goldschmied showed the benefits of using an integrated boundary layer control and propulsion system and proposed using a thick-wing concept with embedded blowers [3]. Even without considering boundary layer ingestion, Ko estimated that for a blended-wing-body aircraft with embedded propulsion, the propulsive efficiency could be increased from about 80 to 90% [4].

In addition to increased propulsive efficiency, embedded propulsion provides reduced noise and increased safety, because the propulsor is now buried within the structure of the aircraft (e.g., no exposed propellers). Also, based on the methods in [5], by eliminating the engine pylon/nacelle support structure, the aircraft parasite drag can be reduced by up to 18–20%, thus improving cruise efficiency and range. A detailed discussion of the benefits of embedded distributed wing propulsion, as well as both past and present attempts to integrate such a system within an aircraft, is given in [6].

The authors are not the first to propose the use of wing embedded crossflow fans in aircraft. Dornier patented the design of an aircraft that used crossflow fans embedded within the middle of a conventional airplane wing [7]. Hancock proposed distributing fully embedded crossflow fans near the trailing edge of a conventional transport aircraft, with shafts and couplings connecting them to wing-tip and root-mounted gas turbines [8]. Air is ducted into the fan from both wing surfaces and expelled out at the trailing edge. This design, however, limits the fan size and ducting. Also, the CFF may not be a viable option for high-speed applications due to compressibility effects (i.e., choking). Chawla performed a series of wind-tunnel tests, which demonstrated the use of a CFF for boundary layer control through boundary layer blowing [9]. This increased the wing C_L by delaying stall at high angle of attack. Subsequent studies attempted to use flow drawn into the fan from the leading edge and expelled over the suction surface to provide both thrust and circulation control [10,11]. These configurations appear to be unsuccessful, however, due to a poor housing design. In addition to propulsion, there is a current effort at the Naval Postgraduate School to use a CFF installed within the fuselage of a small aircraft for vertical lift [12].

We believe that previous studies of crossflow fan propulsive wings fell short of expectations due to both poor fan placement and poor housing design. This resulted in low fan performance, reduced circulation control, and low thrust production. The purpose of this work is to propose a distributed crossflow fan wing design which encompasses all of the previous aspirations: embedded fan/wing propulsion, high propulsive efficiency, low parasite drag, and reduced flow separation at high angle of attack.

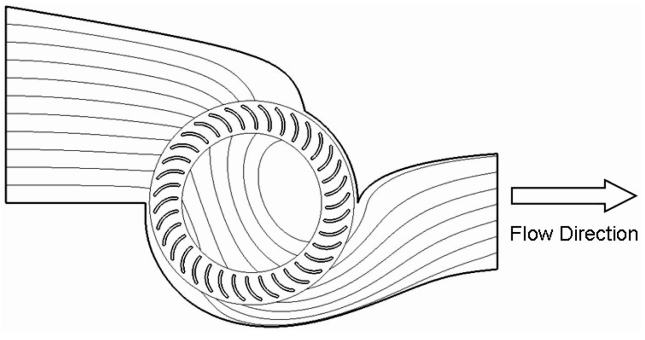

Fig. 2 Baseline inline housing.

II. Crossflow Fan Propulsive Wing Concept

This paper focuses on the application of the crossflow fan to low-speed flight. For an aircraft installation, the propulsor must ingest and expel the flow in a linear manner to produce forward thrust. The conventional HVAC-type CFF housing, characterized by approximately a 90 deg turn from inlet to outlet, is not well suited for this, and as such, an inline fan housing was developed. The baseline inline housing is shown in Fig. 2 and was derived iteratively using the commercial computational fluid dynamics (CFD) software Fluent [13]. The fan rotates counterclockwise as depicted in the figure.

The proposed crossflow fan airfoil design incorporates a partially embedded CFF into a 34% thick modified Gottingen 570 airfoil. Both the inlet and the outlet ducting are located on the suction surface, close to the trailing edge. The design process was again iterative. The CFF airfoil was derived by first embedding the baseline housing within the airfoil section and then adjusting the inlet and outlet ducting to better match the airfoil contours for smooth flow into and out of the fan. In particular, the inlet shape needed to account for the large downward slope of the thick airfoil. Successive CFD runs were necessary to arrive at the final design, shown in Fig. 3. In the figure, the original airfoil geometry is superimposed on the crossflow fan airfoil geometry at what will be considered zero angle of attack.

One concern for many previous investigators was the low total efficiency of the CFF. Published data for fan total efficiency generally lie from 40% for simple geometries to 60% for more complex ones. Mazur in [14] gives a review of previous work in crossflow fan design. Higher total efficiencies in the 70–80% range, however, are documented by Harloff while at the Vought Corporation [15]. The authors are currently investigating the mechanisms by which energy is dissipated in current crossflow fan designs in an effort to improve total efficiency well beyond the 80% mark, bringing the CFF efficiency in line with other forms of propulsion. A full discussion of this topic is outside the scope of this paper and will be reported in the future.

The design of an embedded propulsion system has several challenges that must be addressed. First, by embedding the engines within the wing structure, the fan size becomes restricted. It is well known that axial fans and jet engines incur a large performance penalty as the size reduces. In addition, the embedded engines will inherently ingest highly nonuniform boundary layer flow, which tends to reduce engine performance further [16].

The proposed CFF airfoil will compete well against other propulsion technologies. The raised inlet eliminates the fan size restriction caused by fully embedding the fan within the airfoil. Also, crossflow fan performance is quite insensitive to even large amounts

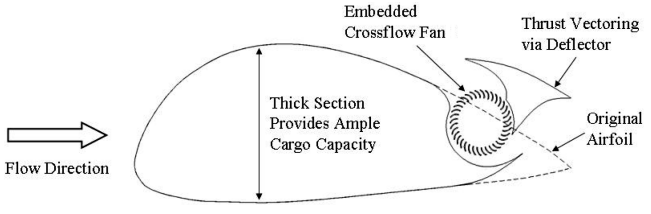

Fig. 3 Crossflow fan airfoil geometry.

of wake ingestion, making it ideal for this type of configuration [17]. In fact, the fan is capable of drawing in the boundary layer, regardless of its thickness. Take, for example, the 34% thick airfoil shown in Fig. 3. Even at a low angle of attack, the wake can be quite large. This renders very thick wing sections impractical for most aircraft applications; the drag penalty outweighs any benefits gained in lift or interior volume. Without the suction effect of the rear-mounted CFF, the flow separates given only a small angle of attack. The embedded crossflow fans near the trailing edge eliminate flow separation by drawing the flow back toward the surface and into the fan ducting, yielding very high-lift coefficients. This in turn results in short takeoff and landing (STOL) capability and low in-flight aircraft stall speed without the use of additional high-lift devices, such as slotted flaps and leading edge slats. In cruise, the low fan efficiency will be offset by lower drag (e.g., engine nacelle, pylon, and interference drag not present). Additionally, the combination of circulation control and differential thrust, accomplished through fan speed and inlet height regulation, may eliminate the need for control surfaces. By vectoring the thrust via a jet flap, additional lifting force and control are also possible.

III. CFD Simulations

The Fluent software package was used to perform CFD simulations of the crossflow fan airfoil. All calculations used the 2-D double-precision segregated solver. Second-order discretization of the convective terms was used throughout all calculations, and the SIMPLE algorithm provided pressure-velocity coupling. The standard k–ε turbulence model was used with the enhanced wall treatment option, which combines a two-layer model with enhanced wall functions for greater robustness in near-wall grid generation (i.e., relaxed requirements on wall y^+ values). To simulate the fan rotating, the area surrounding the blades was designated as a sliding mesh region.

Unsteady simulations require proper setting of both the time step size and the convergence criteria within each time step. For crossflow fan simulations, a time step size equal to 1/20th the blade passing period (e.g., 720 time steps per revolution for a 36-bladed fan) captured the unsteady flow well. Within each time step, iterations were performed until the solution no longer changed. It was found necessary to reduce all residuals (continuity, momentum, and turbulence quantities) to at least 10^{-5}, although for most cases, the residuals were reduced several orders of magnitude less (usually 10^{-7}–10^{-10}). All results in this paper represent time-averaged data over one fan revolution. Dual-CPU Pentium 4 PCs, as well as multiple nodes of a 30-node Beowulf cluster, were used, with the computational time ranging from two days for the housing alone up to two weeks for the full crossflow fan airfoil.

A. Baseline Inline Housing

Before proceeding to integrate the crossflow fan within an airfoil, the baseline inline housing shown in Fig. 2 was simulated independent of the airfoil. During the design process, this allowed for modifications to the internal housing without the added complexity of the external aerodynamics. The domain here was divided into three regions: the flow through the duct, the fan bladed region, and the fan interior. The fan bladed region rotated at a specified rpm, whereas the other two regions remained stationary. A close-up of the grid surrounding the blades is shown in Fig. 4. Quadrilateral mesh was used near the blade surfaces and along the casing walls, and triangular mesh filled in the remainder of the domain. The combination gave a smooth transition from the blade and wall surfaces to the sliding interfaces.

Because no experimental data exist for the current configuration shown in Fig. 2, validation of the CFD model was performed using published results for other housings of *similar shape* [15,18]. The complete CFD study of the fluid mechanics of these crossflow fans, along with validation of CFD results against test data for both global performance quantities (e.g., pressure ratio and efficiency) and detailed flow quantities (e.g., velocity components as a function of angular location at inner and outer fan radii), is presented in [17] and

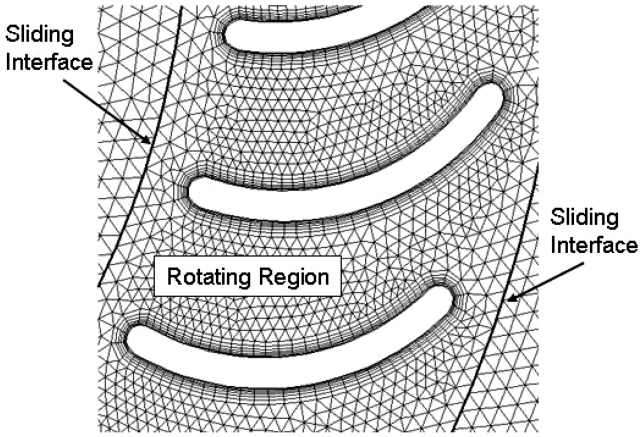

Fig. 4 Close-up of grid near blades.

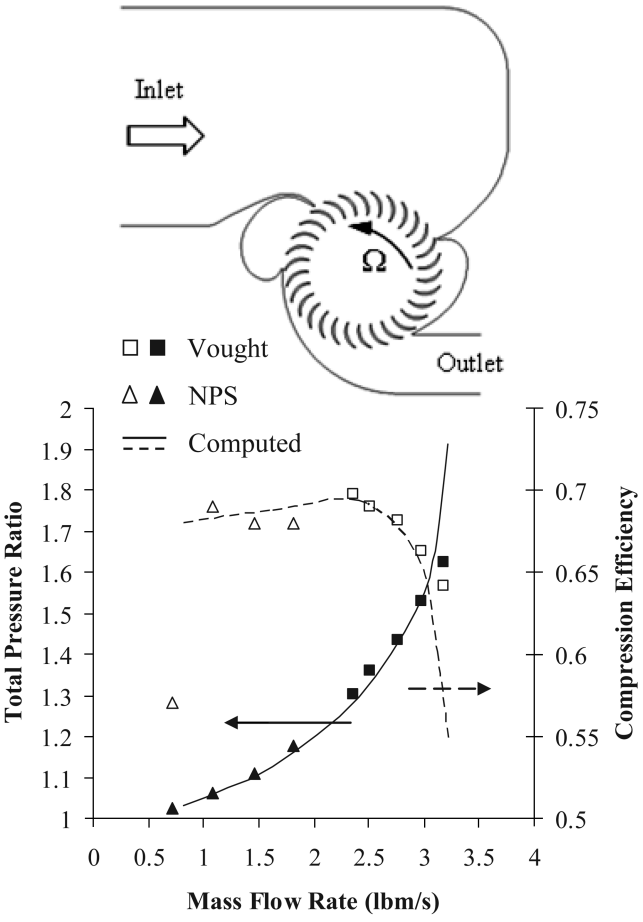

Fig. 5 Performance comparisons: CFD vs experimental results [17].

is outside the scope of this paper. Figure 5 provides a sample of these results (global performance data), where the solid and dashed lines labeled *computed* refer to the CFD results and the symbols correspond to experimental data. The figure shows excellent agreement between CFD and experiment, providing confidence in future crossflow fan simulations. These tests were carried out from low speed to supersonic speed near the choking condition (the maximum relative Mach number in the flow path is on the order of 3.0). Note that the housing geometry used in the experiment is more complicated than the one used in this study (Fig. 2); it includes primary/secondary cavities in the housing, and the blade geometry is of the double circular-arc type which is more efficient at high Mach number. The test data show that the maximum compression efficiency is on the order of 70%, although maximum compression

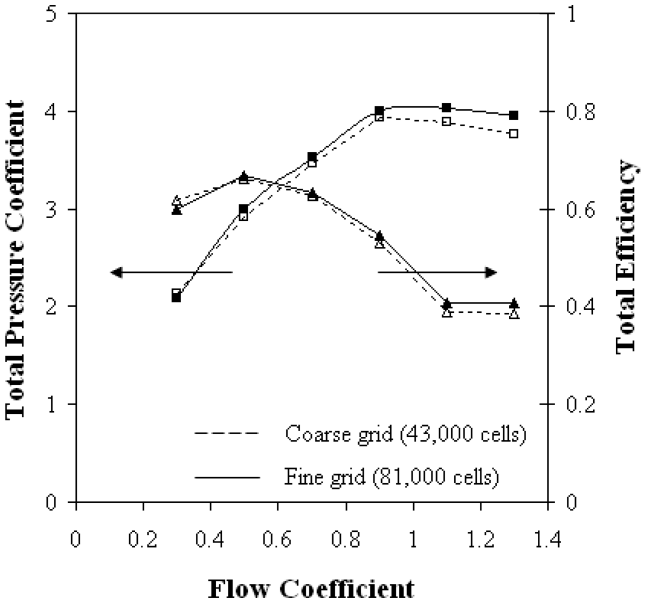

Fig. 6 Computed inline housing fan performance.

efficiency on the order of 80% was demonstrated through CFD simulations by varying the housing design [17].

For the present simulation, a 0.3 m diam 36-blade fan was selected. The blades consisted of simple circular arcs with rounded leading and trailing edges. The inlet and outlet heights were 0.3 m and 0.176 m, respectively. The density and viscosity were set to standard sea level conditions: $\rho = 1.225$ kg/m^3 and $\nu = 1.46 \times 10^{-5}$ m^2/s. At the inlet, uniform ambient total pressure was specified with a turbulence intensity of 1% and hydraulic diameter of 0.3 m. A uniform static pressure boundary condition was specified at the outlet. Changes in mass-flow rate, and hence flow coefficient, were achieved by adjusting the backpressure. The data presented correspond to a fixed fan speed of 2000 rpm and a time step size of 4.17×10^{-5} s.

A grid dependency study was performed, with the final mesh consisting of 81,000 cells. The calculated fan performance for this case is shown in Fig. 6. The figure also gives the results for a coarser grid with only 43,000 cells. The graph shows that using half the grid cells produces only a small change in the results. A common feature of crossflow fans, it is interesting to note that the operating point corresponding to maximum total pressure coefficient does not coincide with that for maximum total efficiency. For the fine mesh, the maximum total pressure coefficient is 4.03 at $\phi = 1.1$; the total efficiency reaches a maximum value of 67% at $\phi = 0.5$. This performance map will be used for our system-analysis model to be discussed later.

B. Crossflow Fan Airfoil

1. *Simulation Setup and Grid Sensitivity*

Simulation of the crossflow fan airfoil takes considerably more time than for the housing alone. The time to reach steady state is based on the flow time from inlet to outlet. As the domain is small, for the baseline housing this occurs after only a few thousand time steps. In contrast, for the CFF-airfoil simulations, the steady state is not reached for many times that number because the computational domain measures $20c \times 20c$, where c is the airfoil chord length. As an example, with the airfoil at zero degree angle of attack and the fan speed set to 1000 rpm, the unsteady calculations took about 24,000 time steps, or about 2 s of flow time, to reach the steady state. The drastic increase in computation time stems from the fact that in the latter case enough time must elapse for the error in the initial solution to convect downstream and out of the domain. The same is true for the housing alone; however, the domain is significantly smaller, allowing the error to propagate out much faster.

The airfoil geometry was given previously in Fig. 3. An airfoil chord length of 15 ft was selected, and the corresponding crossflow fan diameter was 2.1 ft. At the inlet, uniform velocity was specified in the positive x direction with a turbulence intensity of 1% and turbulent viscosity ratio of 5. At the outlet, a uniform static pressure boundary condition was used. Symmetry boundaries were specified for the top and bottom of the domain. It is noted here that although inlet turbulence intensity and turbulence modeling may be important in the case of airfoil-alone computations, especially in predicting accurate stall characteristics, the effect here will be small due to the suction effect of the embedded CFF (i.e., for large suction, the flow over the airfoil approaches an "inviscid" flow). Additionally, 20 chord lengths proved more than adequate for the far-field domain size, especially when the flow direction was strictly left to right (i.e., inlet and outlet flow directions were horizontal, and the airfoil was rotated and remeshed for different angles of attack). Expanding the domain size further, for example, to $50c \times 50c$, produces a negligible change in the lift calculation. Note that if accurate drag count is required, all these effects are likely to be important (e.g., inlet turbulence intensity, turbulence model, far-field location).

Mesh generation was similar to the inline housing case. Quadrilateral mesh covered the blade surfaces and exterior airfoil geometry, and triangular mesh filled in between. Two interfaces were again used: one just outside of the fan blades, and one just inside. To demonstrate solution dependency to mesh changes, the CFF airfoil was simulated at zero degree angle of attack at an altitude of 8000 ft: $\rho = 0.001868$ slug/ft^3 and $\nu = 1.914 \times 10^{-4}$ ft^2/s. The freestream velocity was set to 206 ft/s ($Re = 1.6 \times 10^7$, $M_\infty = 0.19$), and the fan speed to 1000 rpm. The corresponding time step size used was 8.33×10^{-5} s. The starting solution for the unsteady case was obtained by first performing a steady calculation with the fan modeled as a moving reference frame zone. In doing this, the fan region does not rotate; however, the no-slip boundary condition on the fan blades is still enforced in the relative frame (i.e., the local blade velocity is equal to Ωr). This produces a total pressure rise through the fan with magnitude comparable to the unsteady calculation and consequently provides a good initial solution for the external aerodynamics.

The grid dependency study presented consists of three grids of increasing resolution: 64,000 cells, 88,000 cells, and 131,000 cells. The average fan blade y^+ values for the coarse, medium, and fine grids were 63, 46, and 22, respectively. Table 1 gives the final computed results for each grid, along with the percent difference between the fine and the two coarser grids. In the current configuration, the jet leaves the fan with a large amount of swirl, causing the flow to deflect upwards, and resulting in a net downward force on the airfoil (i.e., negative lift coefficient). Based on these results, the fine grid was chosen for the remainder of the CFF-airfoil simulations.

Table 1 Grid comparison at 1000 rpm

	Coarse Grid		Medium Grid		Fine Grid
Parameter	Value	% difference from fine grid	Value	% difference from fine grid	Value
ϕ	0.933	1.7	0.909	−1.0	0.918
Ψ_t	4.260	5.8	4.032	0.1	4.026
η_t	0.547	−1.6	0.555	0.0	0.555
C_L	−0.561	−10.7	−0.604	−3.9	−0.628

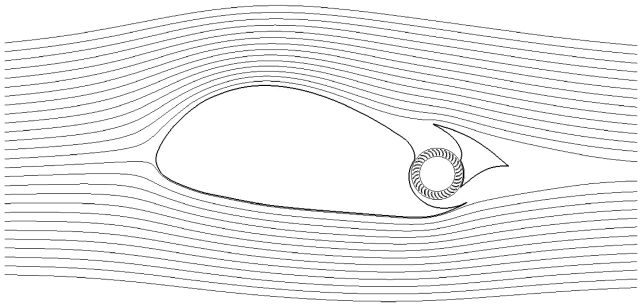

a) Fan off

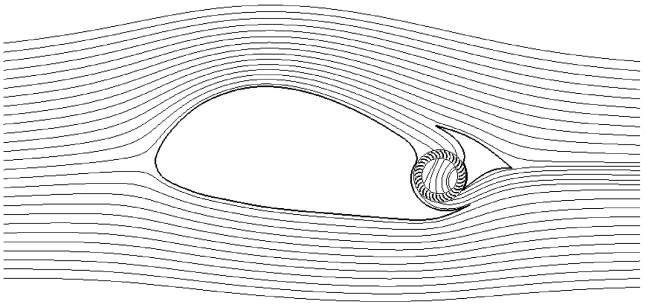

b) Fan on – 1,000 rpm

Fig. 7 Time-averaged streamlines at 10 deg angle of attack.

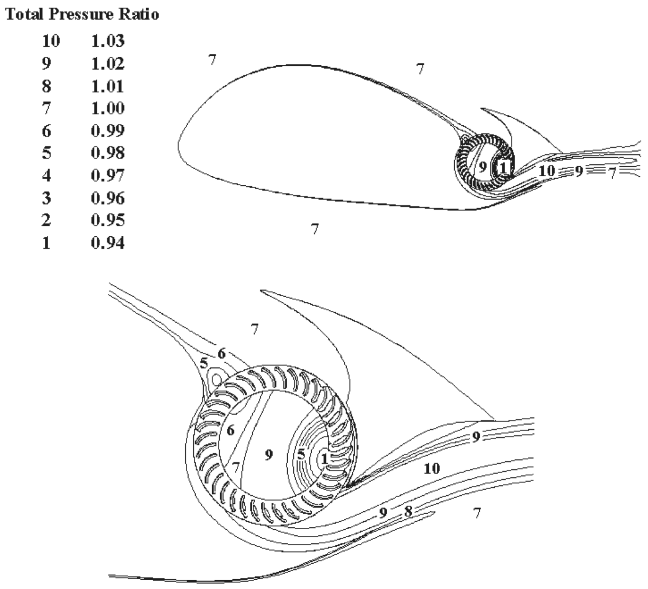

Fig. 8 Total pressure ratio contours at 10 deg angle of attack.

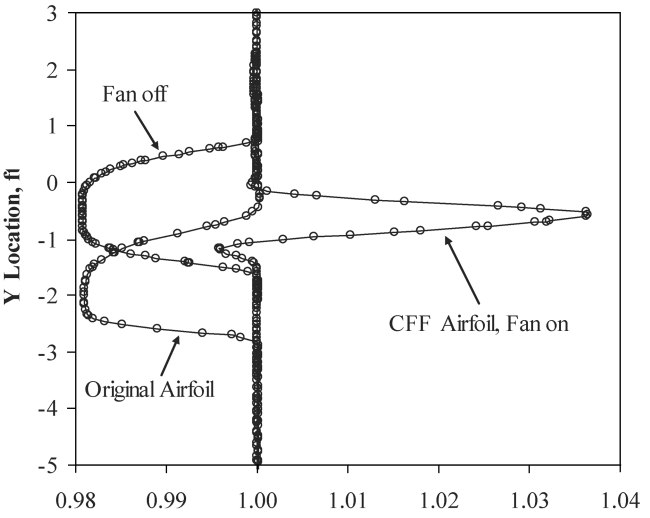

Fig. 9 Total pressure wake profiles.

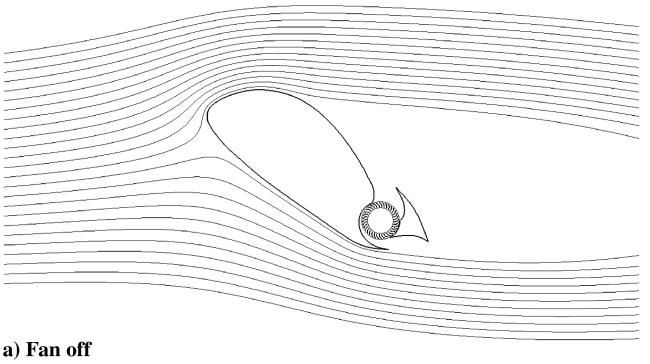

a) Fan off

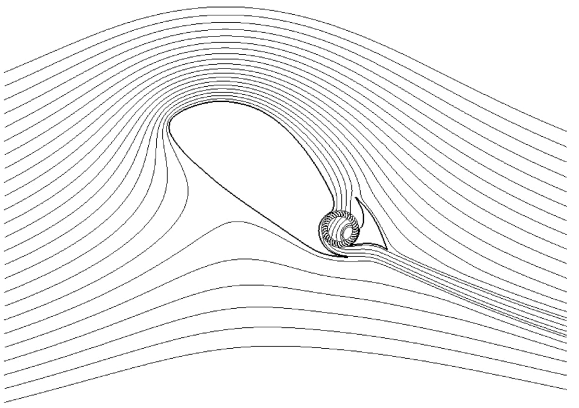

b) Fan on – 1,250 rpm

Fig. 10 Time-averaged streamlines at 40 deg angle of attack.

2. Low Angle of Attack Configuration

The CFF airfoil was next simulated at 10 deg angle of attack at 200 ft/s and standard sea level conditions ($Re = 1.9 \times 10^7$, $M_\infty = 0.18$). The fan speed was again set at 1000 rpm; the time step size remained at 8.33×10^{-5} s. The grid was generated by rotating the airfoil clockwise and reconstructing the grid as done previously. The jet deflector was aligned horizontally to force the flow to leave the CFF ducting in the freestream direction.

Figure 7 shows the streamlines for this case. With the fan off, the flow effectively bypasses the fan ducting, producing a large wake behind the airfoil. With the fan on, however, the wake size reduces dramatically. Total pressure contours with the fan on are given in Fig. 8 and present a clear picture of where energy is gained and lost. The values in Fig. 8 are presented as total pressure ratio, defined as the local total pressure divided by the freestream value. The large values for total pressure ratio in the exhaust correspond to the thrust producing high momentum jet flow, whereas values less than 1.0 represent energy loss. From the figure, the boundary layer growth over the suction surface is apparent. An important feature of the crossflow fan is its ability to operate well even when the inlet profile is nonuniform due to ingestion of low momentum boundary layer flow. Also visible in Fig. 8 is the eccentric vortex, the region of very low total pressure located within the fan.

Figure 9 shows the wake profiles for the 1000 rpm case, for the fan turned off, and for the original airfoil at 10 deg angle of attack. The data are shown along a vertical line 10% chord behind the airfoil. With the fan turned off, the wake profile is very similar to that for the original airfoil alone, only shifted in the vertical direction due to the change in the trailing edge geometry. The large total pressure deficit indicates a substantial wake immediately behind the airfoil. With the

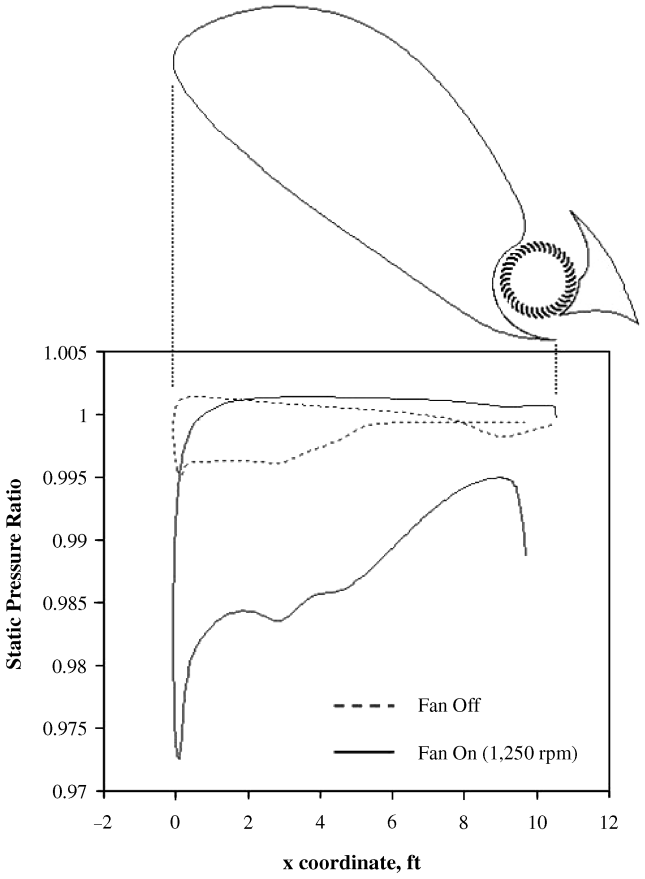

Fig. 11 Static pressure ratio distribution at 40 deg angle of attack.

fan turned on, the total pressure profile outside the jet matches the freestream almost exactly. The jet produces a total pressure increase in the wake region and entrains the flow near the airfoil trailing edge, virtually eliminating boundary layer separation. Additionally, the jet provides excess thrust, which is necessary in practice, since 3-dimensional effects will be present, while at the same time, complete spanwise distribution of the crossflow fan system will probably not be possible.

3. High-Lift Configuration

As mentioned previously, the crossflow fan airfoil is ideal for high-lift STOL applications. To demonstrate this, the airfoil was next placed at 40 deg angle of attack, with a freestream velocity of 50 ft/s at standard sea level conditions ($Re = 4.8 \times 10^6$, $M_\infty = 0.045$). Additionally, to demonstrate the mechanism for vectored thrust, the exit ducting was deflected 30 deg downward.

Figure 10a shows the streamlines with the fan off. As expected, a large area of separated flow is present. The airfoil here is fully stalled, with a calculated lift coefficient of 1.054. This is in stark contrast to the case with the fan turned on. The time-averaged streamlines at 1250 rpm are plotted in Fig. 10b and show that the flow remains fully attached. Also note from Fig. 10 the chordwise movement of the stagnation point from the fan-off to fan-on conditions. This clearly demonstrates the circulation control aspect of the CFF airfoil. The static pressure ratio distribution, defined as the local pressure divided by the freestream value, is given in Fig. 11. In the figure, the leading edge is located at $x = 0$, whereas the crossflow fan inlet is at approximately $x = 9.7$ ft. With the fan off, the flow is fully separated over the suction surface, creating a relatively uniform (and high) pressure along the majority of the chord length. With the fan on, however, there is a strong suction effect, including a large drop in static pressure near the propulsor inlet, which draws the flow into the fan housing. As a consequence, the pressure on the upper airfoil surface decreases significantly, thus demonstrating the large increase in lifting capacity. The computed lift coefficient is 6.408 for the fan-on case. Assuming the engine has enough power, the rpm can always be increased to provide a stronger suction into the fan, effectively creating a stall-free airfoil. The effect will only be limited by the mass-flow rate (i.e., fan choking). It is unlikely, however, that choking will be a problem, since the high-lift configuration would only be used at takeoff and landing, where the freestream Mach number is low, and for low-speed maneuvers. As an example, for the present case, the maximum Mach number is 0.27, located within the fan housing at the second stage (discharge) of the crossflow fan.

4. Summary of CFF-Airfoil Numerical Results

Table 2 provides a summary of the numerical results for the CFF-airfoil simulations at 10 and 40 deg angle of attack. The negative values for drag coefficient indicate a net thrust. Horsepower (HP) was computed using the time-averaged torque on the crossflow fan blades.

IV. Crossflow Fan Airfoil System Analysis

As a preliminary design tool, a system level analysis is presented. The purpose of this formulation is to examine the benefits of embedded crossflow fan propulsion, to investigate the tradeoffs between various design parameters, and to allow for initial sizing of the fan and input power. It is assumed that the aircraft is cruising at a specified altitude and speed, and that the fan performance curves are given. CFD results will be used to validate the model.

A. System-Analysis Model

To adequately model the proposed CFF-airfoil configuration, several important features must be included. As already demonstrated by the preceding CFD results, the propulsion system ingests a large amount of boundary layer, or wake, flow from the airfoil suction surface. Inlet momentum deficit does not strongly affect CFF performance; however, it does play a major role at the system level. In the current design, the flow exits the propulsor at the trailing edge as a jet and fills up the wake behind the airfoil. As mentioned previously, this too has a positive effect and hence must be included in the model. Finally, and probably most importantly, the crossflow fan itself must be modeled.

The proceeding analysis is based on the model given in Fig. 12. The inlet velocity profile is given by $U_w(y)$, and the inlet height by h_i. The flow accelerates through the propulsor and leaves with velocity U_j. Ambient static pressure is assumed at both the inlet and the outlet. For low-speed applications, this is usually a good approximation at the outlet, but will not be correct at the inlet, since the pressure is inherently different due to airfoil curvature (i.e., potential field effects). In the design process, one needs to consider this when sizing the inlet. Likewise, when making comparisons with experimental or CFD results, the inlet velocity must be converted to an equivalent profile corresponding to the same total pressure, but at ambient static pressure.

Table 2 Summary of numerical results

Angle of attack, deg	C_L	C_D	ϕ	Ψ_t	η_t	HP per foot of span
10, fan off	0.423	0.035	——	——	——	——
10, fan on −1000 rpm	0.543	−0.056	0.943	4.544	0.550	46.964
40, fan off	1.054	0.225	——	——	——	——
40, fan on −1250 rpm	6.408	−0.987	0.506	2.337	0.601	23.167

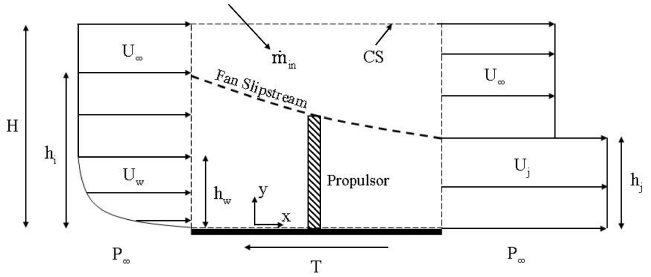

Fig. 12 Model for system analysis with wake ingestion.

Using conservation of mass and conservation of momentum in the x direction, given in Eqs. (1) and (2), respectively, propulsor thrust and inlet momentum deficit, termed here boundary layer drag, are determined.

$$\int_{\mathrm{CS}} \boldsymbol{U} \cdot d\boldsymbol{A} = 0 \tag{1}$$

$$F_x = \rho \int_{\mathrm{CS}} U_x(\boldsymbol{U} \cdot d\boldsymbol{A}) \tag{2}$$

For the present model, a constant jet velocity was assumed ($U_j = \text{const}$). At the inlet, a power-law relation was used, since when compared to the CFD results, this was found to give a good approximation to the mass-flow rate with wake ingestion. The inlet profile is given in Eq. (3), where p is yet to be determined.

$$U_w = \begin{cases} U_\infty (y/h_w)^p & \text{for } 0 \le y \le h_w \\ U_\infty & \text{for } h_w < y \le h_i \end{cases} \tag{3}$$

For a control volume spanning from far upstream to the propulsor inlet, inserting Eq. (3) into Eqs. (1) and (2) and integrating yields the boundary layer drag.

$$D_{\mathrm{BL}} = \rho U_\infty^2 h_w \left[\frac{1}{p+1} - \frac{1}{2p+1} \right] \tag{4}$$

Performing a similar calculation for the control volume shown in Fig. 12 between the inlet and outlet yields the thrust.

$$T = \rho U_\infty (U_j - U_\infty) \left[\frac{h_w}{p+1} + (h_i - h_w) \right] + \rho U_\infty^2 h_w \left[\frac{1}{p+1} - \frac{1}{2p+1} \right] \tag{5}$$

Dividing Eq. (4) by Eq. (5) gives the ratio of ingested boundary layer drag to thrust. This quantity ranges from zero, corresponding to no wake ingestion (or infinitely large thrust), to one (exhaust velocity equal to freestream velocity), and is a convenient means for comparing different designs. In Eq. (6) $\tilde{h}$ is the ratio of the ingested wake height to the inlet height and also ranges from zero to one. It is important to note that a small value for $\tilde{h}$ may correspond to either minimal wake ingestion (for a fixed inlet height) or a large inlet height (for a fixed wake ingestion).

$$\frac{D_{\mathrm{BL}}}{T} = \frac{1}{\frac{(\tilde{U}_j - 1)[1/\tilde{h} + 1/(p+1) - 1]}{1/(p+1) - 1/(2p+1)} + 1} \tag{6}$$

where

$$\tilde{h} = h_w / h_i \tag{7}$$

The crossflow fan is modeled by bringing in the fan performance map. This is accomplished by using either CFD or experimental data for a particular design, or by using a "nominal" performance map, corresponding to configurations very similar to the present application. This is possible, since it was found that alterations in the baseline inline housing geometry for installation purposes produce only minor changes in the fan performance.

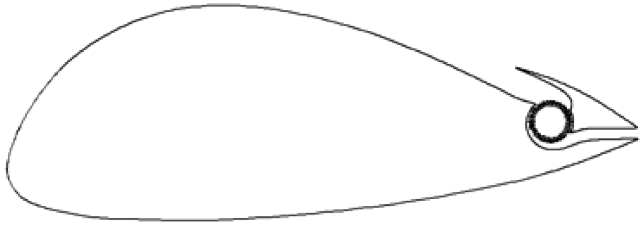

Fig. 13 Modified CFF airfoil with 1.0 ft diam fan.

To bridge the gap between the exterior analysis and the fan performance curves, it is necessary to match the total pressure rise through the propulsor. Here, the mass-weighted total pressure is used at the inlet

$$\bar{P}_{T_i} = \frac{\int_0^{h_i} P_{T_i}(y) d\dot{m}}{\int_0^{h_i} d\dot{m}} \tag{8}$$

Of particular interest are the quantities relating propulsor thrust to the kinetic energy input to the flow and the power input to the fan. The first is called propulsive efficiency, and is defined in Eq. (9).

$$\eta_p = \frac{TU_\infty}{P_P} \tag{9}$$

where

$$P_p = \frac{1}{2}\rho \int_0^{h_j} U_j^3 dy - \frac{1}{2}\rho \int_0^{h_i} U_w^3 dy \tag{10}$$

Substituting Eqs. (5) and (10) into Eq. (9)

$$\eta_p = \frac{2(\tilde{U}_j - 1)\left[\frac{\tilde{h}}{p+1} + (1 - \tilde{h})\right] + 2\tilde{h}\left[\frac{1}{p+1} - \frac{1}{2p+1}\right]}{(1 - \tilde{h})(\tilde{U}_j^2 - 1) + \tilde{U}_j^2 \frac{\tilde{h}}{p+1} - \frac{\tilde{h}}{3p+1}} \tag{11}$$

Nondimensionalizing thrust and power, the second relation, given by Eq. (12), represents the amount of thrust produced per unit power. By maximizing this quantity, for a given thrust, the necessary power input will be minimized.

$$\frac{C_T}{C_P} = \frac{4\eta_t \mu^2}{\Psi_t} \left[(\tilde{U}_j - 1) + \frac{\frac{\tilde{h}}{p+1} - \frac{\tilde{h}}{2p+1}}{1 - \tilde{h} + \frac{\tilde{h}}{p+1}} \right] \tag{12}$$

where μ is the advance ratio, and is related to the flow coefficient through the relation

$$\phi = \mu \frac{h_i}{D_f} \left[1 - \tilde{h} + \frac{\tilde{h}}{p+1} \right] \tag{13}$$

The system-analysis formulation thus involves evaluating the effect of the three independent parameters μ, $\tilde{h}$, and h_i/D_f, on the overall measures of system performance: D_{BL}/T, C_T/C_P, and η_p.

B. CFF-Airfoil Simulations for Comparison

To proceed further, it was first necessary to determine the value of the exponent p in the preceding analysis. This parameter defines the typical shape of the inlet boundary layer profile. In addition, to validate the model, comparison runs were needed. As test data were not available, CFD simulations of the baseline inline housing and CFF airfoil were used for these tasks. For the CFF airfoil, two different geometries were run. The first corresponded to Fig. 3, where the chord length was 15 ft and the crossflow fan diameter was 2.1 ft. Calculations were performed for seven different rpm settings at zero degree angle of attack with fan speeds ranging from 500 to 1250 rpm. The second set of runs corresponded to approximately the same exterior airfoil shape, but with a 1.0 ft diam fan included. This modified geometry is shown in Fig. 13. The objective here was to produce approximately the same thrust when using the small fan as

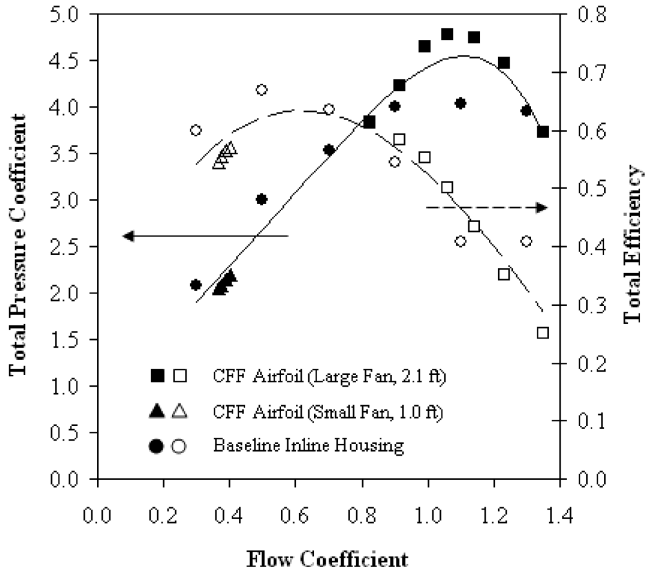

Fig. 14 Crossflow fan performance.

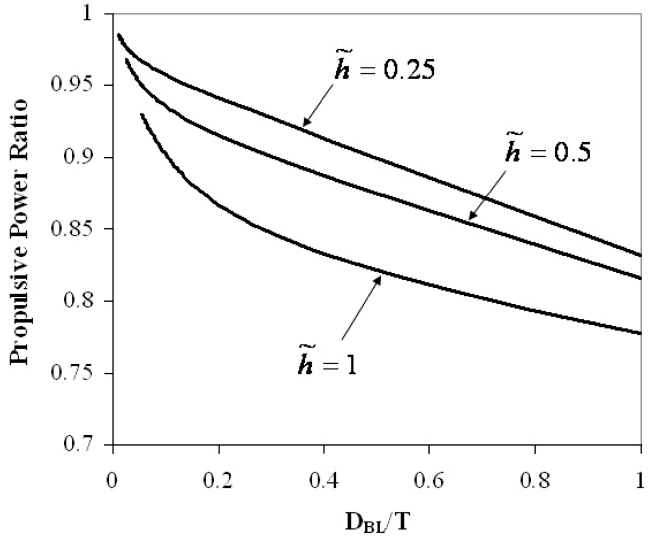

Fig. 15 Effect of boundary layer ingestion on propulsive power ratio for $h_i/D_f = 0.5$.

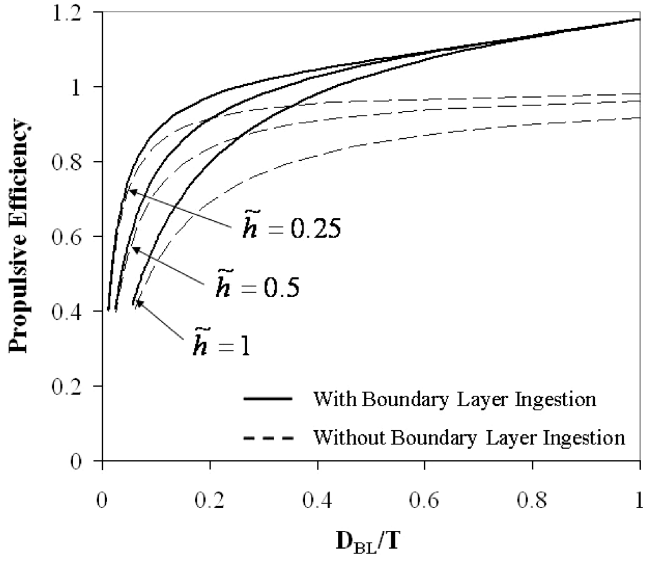

Fig. 16 Effect of boundary layer ingestion on propulsive efficiency for $h_i/D_f = 0.5$.

was found previously for the larger one, and thus the fan speed needed to be much higher. For this case, calculations were performed at four fan speed settings ranging from 3000 to 6000 rpm.

A compilation of the fan performance data for all three cases is given in Fig. 14. The solid and dashed lines plotted in Fig. 14 are polynomial curve fits for total pressure coefficient and total efficiency, and are given by Eqs. (14) and (15), respectively. The curves show good agreement between the three cases over the range of flow coefficients simulated. By using curve-fitted data, the complexity of the proceeding analysis is reduced by allowing the fan performance for all cases to be approximated by a single set of curves. Additionally, by adjusting the value of p, it was found that the best match for mass flow rate across all cases between the CFD data and the boundary layer profile given in Eq. (3) was for $p = 0.28$, with an average error of less than 0.3%.

$$\Psi_t = -5.3731\phi^4 + 11.166\phi^3 - 8.3403\phi^2 + 6.5663\phi + 0.4212 \tag{14}$$

$$\eta_t = 0.2898\phi^3 - 1.3829\phi^2 + 1.3682\phi + 0.2479 \tag{15}$$

C. Results

The current model includes boundary layer ingestion into the fan, whereas in the conventional propulsion model, the propulsor ingests only uniform freestream flow. From [2], the thrust, propulsive power, and propulsive efficiency for the latter case are

$$T' = \dot{m}'_j(U'_j - U_\infty) \tag{16}$$

$$P'_p = \tfrac{1}{2}\dot{m}'_j(U'^2_j - U^2_\infty) \tag{17}$$

$$\eta'_p = \frac{2}{\tilde{U}'_j + 1} \tag{18}$$

where the primed quantities correspond to the nonwake ingestion case.

For comparison, two propulsors with equal thrust and mass flow rate will be used: one with and one without boundary layer ingestion. Dividing Eq. (10) by Eq. (17) yields the propulsive power ratio, which represents the energy savings relative to the conventional nonwake ingestion case.

$$\frac{P_p}{P'_p} = \frac{(1-\tilde{h})(\tilde{U}_j^2 - 1) + \tilde{U}_j^2\frac{\tilde{h}}{p+1} - \frac{\tilde{h}}{3p+1}}{(\tilde{U}'^2_j - 1)\left[\frac{\tilde{h}}{p+1} + (1-\tilde{h})\right]} \tag{19}$$

where

$$\tilde{U}'_j = \tilde{U}_j + \left[\frac{\frac{1}{p+1} - \frac{1}{2p+1}}{\frac{1}{p+1} + \frac{1}{\tilde{h}} - 1}\right] \tag{20}$$

Propulsive power ratio and propulsive efficiency are plotted in Figs. 15 and 16 versus D_{BL}/T for $h_i/D_f = 0.5$. In the figures, small values of D_{BL}/T correspond to large thrust production, whereas $D_{BL}/T = 1$ corresponds to a perfect filling in of the wake behind the airfoil (i.e., the ideal cruising condition). As D_{BL}/T and $\tilde{h}$ increase, propulsive power ratio decreases. The greatest power savings is thus achieved when $D_{BL}/T = 1$ and $\tilde{h} = 1$ (i.e., boundary layer ingestion is large). Propulsive efficiency also increases with increasing D_{BL}/T and is always greater with boundary layer ingestion. In accordance with the work by Smith, propulsive efficiency can actually exceed 100% as D_{BL}/T approaches unity [2]. It is interesting to note, however, that as $\tilde{h}$ increases, η_p actually decreases. This is a direct result of the fact that this analysis compares different designs of equal thrust. At a given value of D_{BL}/T (i.e., a fixed boundary layer ingestion height h_w), as $\tilde{h}$ increases, the propulsor size decreases, resulting in reduced mass flow. In turn, as the mass flow rate decreases, the necessary power which must be imparted on the flow

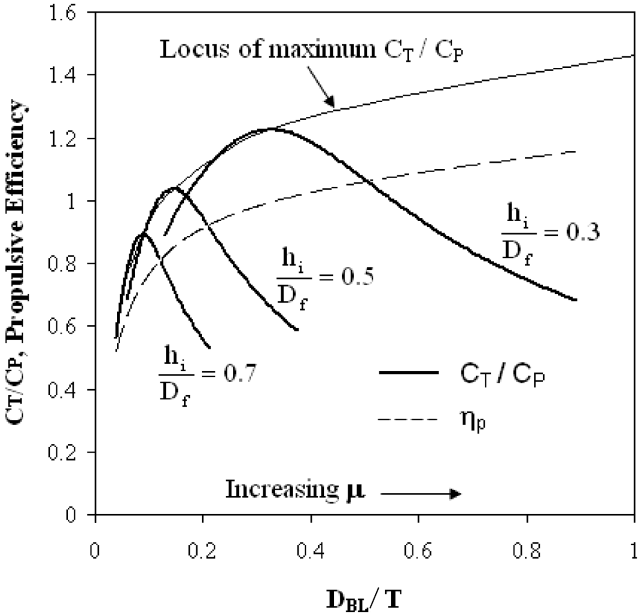

Fig. 17 Variation in h_i/D_f for $\tilde{h} = 0.5$.

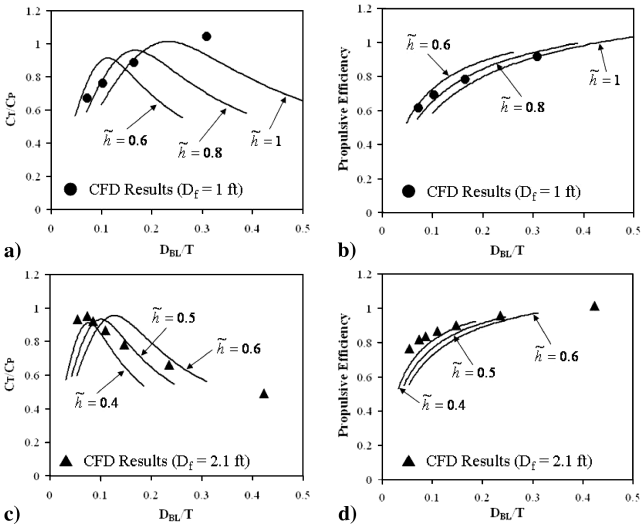

Fig. 18 Comparison between system analysis and CFD results.

to produce a specified amount of thrust (i.e., the propulsive power) increases, thus decreasing propulsive efficiency. For small values of D_{BL}/T, the effect becomes quite significant and implies that for a specified boundary layer ingestion and propulsor thrust, from a propulsive efficiency standpoint, it is desirable to have a large inlet opening. The implication of these results is that, although small propulsors benefit greatly from boundary layer ingestion, larger ones may still result in better performance. Thus a design tradeoff exists where using a larger fan results in higher propulsive efficiency, but with an added weight penalty and greater drag due to an increase in surface area.

The next question is that if $\tilde{h}$ is fixed, for example, at 0.5, is it beneficial to operate at a high or low value of h_i/D_f? This situation is plotted in Fig. 17, which shows that the answer depends on the particular design and operating point. For a fixed value of $\tilde{h}$, a lower h_i/D_f always gives a higher possible value for C_T/C_P. The analysis shows that for a fixed inlet height (i.e., fixed h_i), the best choice for the fan diameter depends on the value of D_{BL}/T; for a given D_{BL}/T, the fan and housing should be chosen such that the operation lies on the maximum C_T/C_P line. For a given wake height, this translates into a direct relation between the necessary thrust and fan diameter for minimum power. Also note, as can be seen in the equations, propulsive efficiency is not a function of h_i/D_f.

To validate the system-analysis formulation, comparisons were made with the CFF-airfoil CFD results. The graphs of C_T/C_P and η_p versus D_{BL}/T for both the small and large fan cases are shown in Fig. 18. Excellent agreement is seen between the system-analysis predictions and CFD data for propulsive efficiency. For C_T/C_P the system analysis also performs well, especially for the larger fan. It is important to note that the comparison depends heavily on an accurate approximation of the wake height $\tilde{h}$. This should come as no surprise, because it was already seen that large amounts of propulsor wake ingestion create notable differences in overall system performance.

As noted previously, it is necessary to compare the analysis with CFD results where the inlet velocity profile is converted to an equivalent one, but at ambient static pressure. In doing this, one also must assume an isentropic contraction or expansion of the flow, depending on whether the pressure is above or below the ambient value. Thus not only is an equivalent velocity profile determined, but also an equivalent inlet height. The level of agreement between the analytical and CFD results is quite good, given that the system-analysis curves correspond to the actual ratio of inlet height to fan diameter (i.e., the physical value of h_i/D_f). If the exact profile for pressure is known at the outset, then even better correlation can be expected. The implication here is that for preliminary design, where the process is reversed, the system analysis will provide a good approximation of the expected performance for a large range of designs, given only a small number of input parameters.

V. Conclusion

A new high-lift propulsive airfoil design was proposed that utilized an embedded crossflow fan for both propulsion and flow control. To facilitate the development of a propulsive crossflow fan airfoil, an inline CFF housing was designed and integrated into a modified Gottingen 570 airfoil. In the design, flow was drawn into the propulsor from the airfoil suction surface and exhausted out at the trailing edge.

To show the benefits of the proposed design, the crossflow fan airfoil was simulated at low and high angles of attack. The fan ingested the boundary layer which built up over the airfoil suction surface, energized this boundary layer flow, and the jet expelled out the trailing edge filled in the wake. This combination resulted in a low drag, high propulsive efficiency design. Angles of attack up to 40 deg were simulated, with the results showing virtual elimination of flow separation and computed lift coefficients greater than 6.

Through a system analysis of the crossflow fan airfoil, propulsive efficiencies greater than unity were found to be possible. Additionally, an important design tradeoff was identified between propulsive efficiency and fan size for minimum power. For the configuration studied, it was found that small propulsors benefit greater from boundary layer ingestion; however, in general, increasing fan diameter improves propulsive efficiency, but at the cost of additional weight and skin friction drag.

From the results presented, several additional conclusions can be drawn:

1) By creating an integrated fan/airfoil system, the interference effects caused by external propulsors and their support structures may be eliminated, increasing overall performance.

2) The high propulsive efficiency and low drag in cruise may provide for increased range over conventional designs.

3) The design readily allows for the mounting of multiple fans along the span of the aircraft. This redundancy improves safety dramatically in the case of fan failure.

4) The distribution of crossflow fan airfoil sections along the entire span lends itself directly to flying wing or blended-wing-body (BWB) type aircraft. By coupling the crossflow fans with individual fuel cell powered electric motors, the need for shafts connecting the fans is eliminated. Such an aircraft provides a platform for a future BWB-CFF aircraft: low emission, low noise, redundant power source, highly efficient in cruise, highly maneuverable, and with excellent STOL capabilities. In the center region of the aircraft, the crossflow fans produce the main thrust, with the thick airfoil sections providing ample room for passengers (e.g., a 34% thick airfoil with a 15 ft chord length has a maximum thickness of over 5 ft). Outboard

airfoil sections will most likely be thinner, but could still contain crossflow fans for added thrust, wake reduction, and control via differential thrust (for yaw control) and differential lift through circulation control and vectored thrust (for roll control).

Acknowledgments

This research was partially funded under the NASA NRA-01-GRC-04 Phase 2 contract, "Revolutionary Aeropropulsion and Power, Concepts, and Technology." The authors would like to thank H. D. Kim, L. Burkardt, and the rest of the systems group at NASA Glenn Research Center for their support and direction throughout the course of this work. Also, the authors would like to acknowledge Fluent, Inc., for providing the CFD software used in this research project.

References

[1] Lazzarotto, L., Lazzaretto, A., and Martegani, A. D., "On Cross-Flow Fan Similarity: Effects of Casing Shape," *Journal of Fluids Engineering*, Vol. 123, Sept. 2001, pp. 523–531.

[2] Smith, L. H., "Wake Ingestion Propulsion Benefit," *Journal of Propulsion and Power*, Vol. 9, No. 1, 1993, pp. 74–82.

[3] Goldschmied, F. R., "Thick-Wing Spanloader All-Freighter: Design Concept for Tomorrow's Air Cargo," AIAA 90-3198, Sept. 1990.

[4] Ko, Y.-Y. A., "The Multidisciplinary Design Optimization of a Distributed Propulsion Blended-Wing-Body Aircraft," Ph.D. Dissertation, Virginia Polytechnic Institute and State University, Blacksburg, VA, 2003.

[5] Roskam, J., and Lan, C.-T. E., "Airplane Drag," *Airplane Aerodynamics and Performance*, Design, Analysis and Research Corporation, Lawrence, KS, 1997, pp. 137–199.

[6] Kim, H. D., and Saunders, J. D., "Embedded Wing Propulsion Conceptual Study," NASA NASA/TM-2003-212696, 2003.

[7] Dornier, P., "Multiple Drive for Aircraft Having Wings Provided With Transverse Flow Blowers," U.S. Patent No. 3,065,928, filed 27 Nov. 1962.

[8] Hancock, J. P., "Test of a High Efficiency Transverse Fan," AIAA Paper AIAA-80-1243, 1980.

[9] Chawla, K., "Optimization of Cross Flow Fan Housing for Airplane Wing Installation," M.S. Thesis, University of Texas at Arlington, Arlington, TX, 1984.

[10] Lin, C.-H., "A Wind Tunnel Investigation of the External Aerodynamics of an Airfoil with an Internal Cross Flow Fan," M.S. Thesis, University of Texas at Arlington, Arlington, TX, 1986.

[11] Nieh, T.-W., "The Propulsive Characteristics of a Cross Flow Fan Installed in an Airfoil," M.S. Thesis, University of Texas at Arlington, Arlington, TX, 1988.

[12] Gossett, D. H., "Investigation of Cross Flow Fan Propulsion for a Lightweight VTOL Aircraft," M.S. Thesis, Naval Postgraduate School, Monterey, CA, Dec. 2000.

[13] Fluent, Software Package, Ver. 6.2, Lebanon, NH, 2003.

[14] Mazur, J. S., "A Study of the Cross Flow Fan," Ph.D. Dissertation, Wayne State University, Detroit, MI, 1984.

[15] Harloff, G. J., "Cross-Flow Fan Experimental Development and Finite-Element Modeling," Ph.D. Dissertation, University of Texas at Arlington, Arlington, TX, 1979.

[16] Daggett, D. L., Kawai, R., and Friedman, D., "Blended Wing Body Systems Studies: Boundary Layer Ingestion Inlets with Active Flow Control," NASA NASA/CR-2003-212670, 2003.

[17] Kummer, J. D., and Dang, T. Q., "Design and Simulation of an Embedded Cross-Flow Fan Propulsive Airfoil," NASA CR NAS 3-03084, 2005.

[18] Cheng, W. T., "Experimental and Numerical Analysis of a Crossflow Fan," M.S. Thesis, Naval Postgraduate School, Monterey, CA, Dec. 2003.